HHS Public Access

Author manuscript

Cancer Res. Author manuscript; available in PMC 2016 April 15.

Published in final edited form as:

Cancer Res. 2015 April 15; 75(8): 1682–1690. doi:10.1158/0008-5472.CAN-14-1855.

Induction of vasculogenic mimicry overrides VEGF-A silencing and enriches stem-like cancer cells in melanoma

Caroline I. Schnegg, **Moon Hee Yang**, **Subrata K. Ghosh**, and **Mei-Yu Hsu***

Department of Dermatology, Boston University Medical Center, Boston, MA 02118

Abstract

The basis for resistance to VEGF inhibition is not fully understood despite its clinical importance. In this study, we examined the adaptive response to VEGF-A inhibition by a loss-of-function analysis using plasmid-based shRNA. Tumor xenografts that initially responded to VEGF-A inhibition underwent an adaptation *in vivo* leading to acquired resistance. VEGF-A blockade in tumors was associated with HIF-1α expression and an increase in $CD144^+$ vasculogenic mimicry (VM), leading to formation of channels displaying Tie-1 and MMP-2 upregulation. $CD133^+$ and $CD271^+$ melanoma stem-like cells (MSLC) accumulated in the perivascular niche. Tumor xenografts of melanoma cell populations that were intrinsically resistant to VEGF-A blockade did not exhibit any of these features, compared to non-target control counterparts. Thus, melanomas which are initially sensitive to VEGF-A blockade acquire adaptive resistance by adopting VM as an alternate angiogenic strategy, thereby enriching for deposition of MSLC in the perivascular niche through a HIF-1α-dependent process. Conversely, melanomas which are intrinsically resistant to VEGF-A blockade do not show any evidence of compensatory survival mechanisms that promote MSLC accumulation. Our work highlights the potential risk of anti-VEGF treatments owing to a selective pressure for an adaptive resistance mechanism that empowers the development of stem-like cancer cells, with implications for how to design combination therapies that can improve outcomes in patients.

Keywords

CD133; CD144; CD271; perivascular niche; HIF-1α

Introduction

Human malignant melanoma is a highly aggressive cancer due to its ability to metastasize and its resistance to conventional anti-cancer treatments. Angiogenesis supports melanoma tumor growth and metastasis by supplying the tumor with oxygen and nutrients and providing tumor cells with an entry route into circulation (1). Given that the key proangiogenic factor is considered to be VEGF-A, anti-VEGF therapies for the treatment of melanoma have been studied extensively (2, 3). Unfortunately, despite showing initial anti-

*Corresponding author: Department of Dermatology, Boston University Medical Center, 609 Albany St., J-410, Boston, MA 02118. Phone: 617-638-5557; Fax: 617-638-5515; meiyuhsu@bu.edu.

Disclosure of Potential Conflict of Interest: No potential conflicts of interest were disclosed.

tumor effects in a subset of patients, anti-VEGF strategies achieved limited efficacy in patients due to the rapid development of resistance (3–6). This adaptive resistance is associated with increased invasion and metastasis of cancer cells (6).

It has long been speculated that in order to escape anti-VEGF therapies, tumors may employ alternative vascularization mechanisms, including vasculogenic mimicry (VM) (7–9). VM is a phenomenon in which tumor cells mimic endothelial cells by undergoing transendothelial differentiation, characterized by their increased expression of vascular markers, such as CD144 (VE-cadherin), EphA2, Tie-1, and MMP-2 (10–13). VM channels provide an alternate mechanism for nutrient supply and act as a potential access point for metastases, and thus correlate with tumor aggressiveness and patient mortality (10). Gene expression analysis has revealed that VM-engaging melanoma subsets express genes associated with undifferentiated embryonic-like cells, suggesting the participation of melanoma stem-like cells (MSLCs) with the phenotypic plasticity to serve an endothelial function (8–18). In agreement with these findings, we previously demonstrated that $CD133^+$ MSLCs colocalize to $CD144^+$ VM-engaging melanoma subsets in a perivascular MSLC niche (19). Thus, in response to VEGF inhibition, MSCLs with the intrinsic ability to differentiate and form VM channels may be selected. While experimental evidence to validate this proposal is limited, treatment of human breast cancer xenografts with bevacizumab, an anti-VEGF antibody, resulted in an increase in the cancer stem-like cell population (20). Furthermore, Wang *et al*. showed that blocking VEGF-A or its receptor, VEGFR-2, inhibited the maturation of tumor endothelial progenitors into endothelium, but did not prevent the transendothelial differentiation of $CD133^+$ glioblastoma cells (21).

Despite speculation that VM induction and MSLC maintenance might impact the effectiveness of anti-VEGF therapies, little research supports this claim and the mechanisms of adaptive resistance following VEGF-A inhibition remain largely unknown. In this study, we examined the adaptive response of WM1617, C8161 and A2058 melanoma cell lines to VEGF-A inhibition in the context of VM niche morphogenesis and MSLC subsets. We hypothesized that tumors overcome VEGF-A inhibition by promoting niche morphogenesis through VM induction and MSLC enrichment. Better understanding of the adaptive response to VEGF-A inhibition will provide valuable insights for designing new approaches to treat melanoma through effective combination therapies.

Materials and Methods

Cell Culture

Melanoma cell lines, WM1617, WM983C, 1205Lu (obtained from Dr. M. Herlyn at the Wistar Institute, Philadelphia, PA), and C8161 (a kind gift from Dr. M.J.C. Hendrix at the Stanley Manne Children's Research Institute, Northwestern University, Chicago, IL), and A2058 cells (obtained from ATCC) were cultured as previously described (22). All cell lines were tested within 6 months using the PowerPlex 18D system (Promega BioSciences, San Luis Obispo, CA).

VEGF-A Knockdown (VEGF-A KD) in Melanoma Cells

VEGF-A silencing in WM1617, C8161 and A2058 melanoma cells was achieved by SureSilencing™ shRNA pGeneClip™ plasmids (SABiosciences, Germantown, MD). Lipofectamine 2000 (Invitrogen, Carlsbad, CA) was used according to the manufacturer's protocol. Stable transfectants were selected with 600 μg/ml G418 (Gibco Laboratories, Grand Island, NY) and subsequently subcloned to select the most efficient KD cells. VEGF-A KD (sh1) and VEGF-A KD (sh2) denote two independent shRNA sequences targeting VEGF-A.

ELISA Assay

Cell lysates were extracted in RIPA buffer (Pierce, Rockford, IL) and quantified by a BCA protein assay kit (Pierce) according to the manufacturer's protocol. Equal amounts (100 μg) of protein were subjected to the human VEGF-A ELISA kit (R&D Systems, Minneapolis, MN) according to the manufacturer's instructions. In separate experiments for baseline VEFG-A measurement, tissue culture supernatant was collected from melanoma cells in serum-free medium (5 ml/ 2×10^6 cells over a period of 14 h) and subjected to the human VEGF-A ELISA kit.

Growth Assay

Growth assays were conducted in six-well plates. Cells were plated at the density of 10,000 cells per well. Cells were counted after four, seven, and ten days. Each cell line was plated in triplicate and the experiment was repeated at least three times with consistency. Data presented represent results from one experiment, and data was analyzed using the Student *t* test.

Soft Agar Assay

Three dimensional soft agar clonogenic assays were conducted in six-well plates as previously described (23). Cells were plated at the density of 10,000 cells per well. Colonies with more than five cells were counted in 20 randomly chosen fields (100×) after ten days using an inverted microscope and the percentage of colony formation was calculated. Each cell line was plated in triplicate and the experiment was repeated three times with consistency. The represented data is compiled from the independent repeats, and data was analyzed using the Student *t* test.

Tubule Formation Assay for Vasculogenic Mimicry *in vitro*

Cells were plated at the density of 10,000 cells per well in 96-well plates coated with Matrigel™ (BD Biosciences, San Jose, CA). Luminal area per field (40×) was observed after 24 hours using an inverted microscope and analyzed using Image J software (National Institutes of Health, Bethesda, MD). Each cell line was plated in triplicate, and the data was analyzed using the Student *t* test.

Real-Time Quantitative RT-PCR (qRT-PCR)

RNA from melanoma cells and frozen tumor xenografts was extracted using an RNAeasy kit (Qiagen, Germantown, MD) and reverse transcribed using the SuperScript III® RT cDNA

Synthesis kit (Invitrogen) according to the manufacturer's protocol. Real-time quantitative PCR (qRT-PCR) was performed subsequently on a StepOnePlus™ Real-Time PCR System (Applied Biosystems, Foster City, CA) using human-specific primers. The primer sequences were as follows: CD133 forward 5'-TTCTTGACCGACTGAGAC-3' and reverse 5'-CCAAGCACAGAGGGTCAT-3'; CD144 forward 5'-ATATGTCAGTGATGACTA-3' and reverse 5'-CTTACCAGGGCGTTCAGG-3'; CD271 forward 5'-ACTCACTGCACAGACTCT-3' and reverse 5'-GAAGCTTCTCAACGGCTC-3'; MMP-2 forward 5'-TTTCCATTCCGCTTCCAGGGCAC-3' and reverse 5'-TCGCACACCACATCTTTCCGTCACT-3' (24); Tie-1 forward 5'-CACGACCATGACGGCGAAT-3' and reverse 5'-CGGCAGCCTGATATGCCTG-3' (25); and GAPDH forward 5'-CGACCACTTTGTCAAGCTCA-3' and reverse 5'-AGGGGAGATTCAGTGTGGTG-3'. All samples were run in triplicate and normalized to the housekeeping gene, GAPDH. Data was analyzed using the $2^{-\Delta\Delta Ct}$ method (26).

Western Blotting

Cell lysates and xenograft tissue homogenates were extracted in RIPA buffer (Pierce) and quantified by a BCA protein assay kit (Pierce) according to the manufacturer's protocol. Equal amounts (40–100 μg) of protein were subjected to electrophoresis and transferred to nitrocellulose. Membranes were probed overnight at 4°C with mouse anti-CD133 (Miltenyi Biotech Inc, clone W6B3C1, San Diego, CA) at 1:200, rabbit anti-CD271 (Alomone, Jerusalem, Israel) at 1:1000, rabbit anti-CD144 (Cell Signaling Technology, Danvers, MA) at 1:1000, or mouse anti-beta-actin (Abcam, Cambridge, MA) at 1:5000 followed by probing with the appropriate secondary antibody conjugated to horseradish peroxidase (Jackson Immunoresearch, West Grove, PA). Immunoreactive bands were visualized by SuperSignal West Pico Chemiluminescent Substrate (Pierce). Densitometry measurements were performed using Image J software (National Institutes of Health, Bethesda, MD); beta-actin was used as a loading control.

Melanoma Xenografts and *In Vivo* Tumorigenicity

Mice are maintained under pathogen-free conditions in an American Association for Accreditation of Laboratory Animal Care (AAALAC)-accredited facility at the Boston University Medical Center, under the supervision of the Laboratory Animal Science Center (LASC) and its staff of veterinarians and support personnel. To determine the effects of VEGF-A downregulation on tumorigenicity, 2×10^5 WM1617 or A2058 melanoma cells transfected with control or VEGF-A shRNA constructs were injected subcutaneously in the dorsal skin of each severe combined immune-deficiency (SCID) mouse (CB17; Taconic Laboratory; five mice per condition). In a separate experiment, to ensure the generation of sizable VEGF-A KD xenografts for various analyses, 2×10^6 WM1617, C8161 or A2058 control or VEGF-A KD melanoma cells were injected per mouse (five mice per group). Tumor volume was monitored and determined as the volume of ellipsoid: $4/3\pi$(width/2×length/2×height/2). Statistical analyses were performed using ANOVA. Melanoma xenografts were harvested when tumors reached 1 cm^3. Xenografts were subjected to various analyses, including immunofluorescence, real-time quantitative RT-PCR, and Western Blot analyses.

Immunofluorescence (IF)

Consecutive frozen melanoma xenograft sections were subjected to double indirect immunofluorescence according to standard protocols. The primary antibodies used were rabbit anti-human CD144 (Cell Signaling Technology) at 1:100, biotinylated anti-human CD133 (Miltenyl Biotec Inc.) at 1:20, rabbit anti-human CD271 (Alomone) at 1:100, and rat anti-mouse CD31 (BD Biosciences, San Jose, CA) at 1:50. The secondary antibodies used were FITC-conjugated donkey anti-rabbit IgG (Accurate Chemical & Scientific Corporation, Westbury, NY) at 1:100, FITC-conjugated mouse anti-biotin IgG (Jackson Immunoresearch) at 1:100, and TRITC-goat anti-rat igG (Jackson Immunoresearch) at 1:100. For control, isotype-matched immunoglobins (Vector Laboratories, Burlingame, CA) were used in place of the primary antibody. Sections were mounted with Vectashield containing DAPI (Vector Laboratories) and examined under a Nikon Eclipse E400 microscope (Melville, NY) equipped with FITC and TRITC filters (Nikon, Tokyo, Japan) and a Mercury-100W lamp (Chiu Technical Corporation, Kings Park, NY). Host angiogenesis ($mCD31^+$) and human melanoma-derived VM channels ($hCD144^+$) were quantified as measured by luminal area per field (100×) using Image J software, and data was analyzed using the Student *t* test.

PAS Staining

Dewaxed formalin-fixed and paraffin-embedded (FFPE) 5 μm melanoma xenograft tissue sections were subjected to the Periodic Acid-Schiff (PAS) Kit (Sigma) according to the manufacturer's instructions. The tubular length of VM-like channels per field (200×) was quantified using Image J software, and data was analyzed using the Student *t* test.

PCR Array

RNA from melanoma cells and frozen tumors was extracted using an RNAeasy kit (Qiagen). The RT^2 Profile pathway-focused PCR array specific for human angiogenesis were purchased from SABiosciences. The complete gene lists for the PCR arrays are available on the SABioscience's website (http://www.sabiosciences.com/). Web-based software provided by the supplier was used to analyze the PCR data.

Statistical Analysis

Differences between two groups were analyzed using the Student *t* test. Differences between more than two groups were analyzed by one-way ANOVA. Two-sided P values of less than 0.05 were considered significant.

Results

VEGF-A silencing in melanoma by plasmid-based shRNA

Using ELISA, we screened five melanoma cell lines, including WM1617, WM983C, 1205Lu, A2058, and C8161 cells, for VEGF-A expression. Based on this screening, the amounts of secreted VEGF-A in the tissue culture supernatant (Fig. 1, A left panel) correlate with those of the cytoplasmic fraction in cell lysates (Fig. 1A, right panel), and WM1617, C8161 and A2058 cells exhibited the highest level of VEGF-A expression (Fig. 1A). Thus,

we chose these cell lines to explore the functional role of VEGF-A with regard to tumor growth and niche maintenance. To test the biological significance of VEGF-A, we generated stable VEGF-A knockdown in WM1617, C8161 and A2058 cells using two independent plasmid-based shRNAs (sh1 and sh2). ELISA revealed VEGF-A knockdown at the protein level in WM1617, C8161 and A2058 cells *in vitro* compared to control cells expressing nontarget shRNA (Fig. 1B and Fig. S1A). Quantitative RT-PCR verified downregulation of VEGF-A message levels *in vitro* (Fig. 1C).

VEGF-A KD attenuates WM1617 and C8161 but not A2058 melanoma cell growth *in vitro*

To explore the effect of VEGF-A KD on cell proliferation *in vitro*, we performed 2D growth assays. VEGF-A KD led to a decrease in WM1617 and C8161 cell growth (Fig. 2A and Fig. S1B). In contrast, VEGF-A KD in A2058 cells did not modulate cell growth (Fig. 2A and Fig. S1B). These results highlight the differential effect of VEGF-A KD on cell growth in different melanoma cell lines. In addition to 2D growth assays, we examined anchorage-independent growth using soft agar colony formation assays. VEGF-A KD did not alter soft agar colony formation in WM1617, C8161 or A2058 cells compared to nontarget control cells (Fig. 2B and Fig. S1C). Furthermore, VEGF-A KD did not modulate VM tubule formation *in vitro*, as measured by VM luminal area, in WM1617 ($p=0.490$), C8161 ($p=0.587$) or A2058 ($p=0.118$) cells (Fig. 2C).

VEGF-A KD retards tumorigenicity in WM1617 but not C8161 or A2058 melanoma xenografts

Given that WM1617 VEGF-A KD (sh1), C8161 VEGF-A KD (sh1) and A2058 VEGF-A KD (sh1) cells exhibited the greatest VEGF-A knockdown efficiency, we chose to use these cells for our *in vivo* studies. In two separate tumorigenicity assays in which mice were injected with 2×10^6 (Fig. 3A) 2×10^5 (Fig. S2A) melanoma cells, VEGF-A KD significantly ($p<0.05$) retarded WM1617 tumor growth compared to the nontarget control i*n vivo*. Although growth was delayed, VEGF-A KD xenografts did eventually develop tumors (data not shown). These findings suggest that in the experimental setting WM1617 cells mirror the initial responders in the clinic; i.e., some melanomas are initially sensitive to VEGF-A silencing, but subpopulations of cells eventually develop adaptive resistance and survive (4–6). In contrast, VEGF-A KD did not affect C8161 or A2058 tumor growth *in vivo*, suggesting that C8161 and A2058 cells are intrinsically resistant to VEGF-A silencing and reflect the disease in clinical non-responders to anti-VEGF therapy (Fig. 3A and Fig. S2B). The efficiency of VEGF-A KD was verified in WM1617, C8161 and A2058 xenografts using ELISA (Fig. 3B).

VEGF KD promotes VM and enriches MSLCs in WM1617 but not C8161 or A2058 melanoma xenografts

To explore the biological significance of VEGF-A KD on niche morphogenesis and MSLC homeostasis, we analyzed expression of the VM marker, CD144, and the stem cell markers, CD133 and CD271, in xenografts by real-time qRT-PCR using human-specific primers and by Western Blot analysis. We observed an increase in both the message (Fig. 4A) and protein (Fig. 4B) levels of CD144, CD133 and CD271 in VEGF-A KD WM1617 xenografts

compared to their nontarget control counterparts, suggesting that VEGF-A KD promotes VM and enriches the MSLC phenotype. Interestingly, while we did not observe an increase in CD144 message levels in VEGF-A KD C8161 xenografts compared to their nontarget control counterparts, we did observe an increase in CD133 and CD271 message levels (Fig. 4A); however, VEGF-A KD C8161 xenografts did not exhibit changes in CD144 or CD271 protein levels (Fig. 4B). VEGF-A KD A2058 xenografts did not exhibit changes in CD144, CD133 or CD271 message levels or CD144 or CD271 protein levels (Fig. 4A and 4B). Attempts to examine CD133 in VEGF-A KD C8161 or A2058 xenografts using Western Blot analysis were unsuccessful due to sensitivity issues (Fig. 4B).

Multilabel immunofluorescence (IF) staining confirmed that VEGF-A KD WM1617 xenografts exhibit increased $CD144^+$ VM-like melanoma channel formation as measured by $CD144^+$ luminal area (p=0.0003) (Fig. 5A), while no significant change in mouse $CD31^+$ blood vessel formation was observed (p=0.074) (Fig. 5A). Thus, WM1617 VEGF-A KD xenografts exhibit a significant increase in the percentage of human tumor-derived VM channels ($hCD144^+$) vs. host angiogenesis ($mCD31^+$) (p=0.0003) (Fig 5A). In contrast, VEGF-A KD C8161 xenografts did not display a change in $CD144^+$ VM-like melanoma channel formation (p=0.269), mouse $CD31^+$ blood vessels (p=0.134) or the percentage of human tumor-derived VM vessels vs. host angiogenesis (p=0.417) (Fig. S3A, left panel). VEGF-A KD A2058 xenografts also did not display a change in $CD144^+$ VM-like melanoma channel formation (p=0.946), mouse $CD31^+$ blood vessels (p=0.059) or the percentage of human tumor-derived VM vessels vs. host angiogenesis (p=0.287) (Fig. S3A, right panel). PAS staining further confirmed that VEGF-A KD increases VM channels as measured by tubular length in WM1617 xenografts (p=0.0008), but not in C8161 xenografts (p=0.384) or A2058 xenografts (p=0.624) (Fig. S4). Consistent with these findings, VM-associated genes, such as Tie-1 and MMP-2 were significantly upregulated in WM1617 but not C8161 or A2058 VEGF-A KD xenografts compared to the control xenografts in an angiogenesis pathway-specific qRT-PCR array (data not shown). These results were further validated by qRT-PCR (Fig. 5B and Fig. S3B).

IF staining also confirmed the increase in $CD133^+$ and $CD271^+$ MLSCs in the perivascular niche in close association to $CD144^+$ melanoma cell-lined VM channels in VEGF-A KD WM1617 xenografts (Fig. 5A). No increase in $CD133^+$ or $CD271^+$ MLSCs was observed in VEGF-A KD C8161 or A2058 xenografts (Fig. S3A). Collectively, these data suggest that WM1617 cells, which are initially sensitive to VEGF-A silencing, eventually acquire adaptive resistance and survive through increased VM formation and MSLC enrichment. In contrast, the C8161 and A2058 cells are intrinsically resistant to VEGF-A silencing and, therefore, fail to show adaptive compensatory mechanisms.

WM1617 tumors compensate for VEGF-A KD by VM induction possibly through a HIF-1α-mediated mechanism

Of note, given that numerous studies have demonstrated that HIF-1α regulates VM and the cancer stem cell-like phenotype (27), we observed an increase in HIF-1α in WM1617 VEGF-A KD xenografts but not in A2058 VEGF-A KD xenografts in an angiogenesis pathway-specific qRT-PCR array (data not shown). We verified these results using qRT-

PCR (Fig. 6A and Fig. S3B). Western blot analysis confirmed an increase in HIF-1α protein levels in WM1617 VEGF-A KD xenografts (Fig. 6B). Attempts to examine HIF-1α expression in C8161 and A2058 VEGF-A KD xenografts were unsuccessful due to sensitivity issues.

Discussion

As melanomas are heterogeneous in the clinical setting, some melanomas initially respond to anti-VEGF therapy but eventually develop clinical resistance, the so-called “initial responders”, while other melanomas are intrinsically resistant and do not respond to anti-VEGF therapy (4–6). In accord with frequent clinical relapses in “initial responders” following anti-VEGF treatments, we show that VEGF-A silencing initially inhibits WM1617 melanoma xenograft growth *in vivo*; however, tumors eventually develop adaptive resistance and overcome VEGF-A inhibition. Conversely, mirroring the clinical disease in non-responders to anti-VEGF-A therapy, we found that C8161 and A2058 cells are intrinsically resistant to VEGF-A silencing. Compensatory survival pathways in the initial responders to anti-VEGF therapies have had a negative impact on their clinical effectiveness; however, the mechanisms responsible for the adaptive resistance to anti-VEGF-A therapies are largely unknown. Our studies reveal that VEGF-A inhibition in WM1617 xenografts leads to an increase in $CD144^+$ melanoma cell-lined VM channels and associated VM markers, Tie-1 and MMP-2, providing evidence that VM induction results from an adaptive response to VEGF-A inhibition. C8161 and A2058 xenografts, which were intrinsically resistant to VEGF-A silencing, failed to show adaptive compensatory mechanisms and did not exhibit an increase in VM formation. Taken together, our data suggests that some melanomas develop adaptive resistance to VEGF-A inhibition by increasing VM, an alternate vascularization mechanism to angiogenesis, which is essential in supplying tumors with oxygen and nutrients to support tumor growth (10).

The role of VEGF signaling in regulating VM has been widely studied, however, it remains controversial. Initial reports demonstrated that VEGF-A stimulation did not affect VM (28). Consistent with these reports, VEGF neutralizing antibody Bevacizumab failed to modulate VM formation in glioblastoma cells *in vitro*, and AG28262, a selective inhibitor of VEGFR-1, R-2, and R-3, did not modulate glioblastoma-derived VM channels *in vivo* (29, 30). Conversely, VEGF-A downregulation abolished VM in osteosarcoma cells *in vitro* and VEGFR-2 downregulation reduced VM formation in glioblastoma cells *in vitro* and *in vivo* (30–33). In melanoma, VEGFR-1 expression on melanoma stem-like cells has been shown to promote tumor growth via increased VM formation (34). As stated above, our data demonstrate that VM is increased in some melanomas following VEGF-A inhibition. Such discrepancies of the role of VEGF signaling in modulating VM formation may reflect cell type- and/or cell line-specific differences, and emphasize the importance of the cellular context in determining the response to VEGF-A inhibition.

VM and stem cell signaling pathways are intertwined in the tumor microenvironment (35). Gene expression analysis has revealed that VM-engaging melanoma subsets express genes associated with undifferentiated embryonic-like cells, suggesting the participation of MSLCs with the phenotypic plasticity to serve an endothelial function (10–15, 36).

Furthermore, we previously demonstrated that $CD133^+$ MSLCs colocalize to $CD144^+$ VM-engaging melanoma subsets in a perivascular MSLC niche, and Valyi-Nagy *et al*. showed that VM-forming uveal melanoma cells preferentially express the stem cell marker $CD271^+$ (19, 37). Parallel to these reports, we found that VM induction following VEGF-A inhibition leads to a concurrent increase in $CD133^+$ and $CD271^+$ MSLCs in the perivascular niche of WM1617 xenografts, but not in C8161 or A2058 xenografts, suggesting that some melanomas adapt to VEGF-A inhibition through enrichment of MSLCs, which exhibit the intrinsic ability to differentiate and form VM channels. Highlighting the importance of the microenvironment in supporting VM induction and MSLC maintenance, we did not observe changes in (i) CD144, CD133 or CD271 expression, (ii) VM induction, or (iii) growth in soft agar following VEGF-A knockdown in WM1617 cells *in vitro*. These observations support the view that the dynamic niche microenvironment is imperative in providing the essential cues for cell fate determination, including the phenotypic and functional rendering of VM channels and MSLC enrichment (19, 35, 38–40).

As a result of pruning the tumor vasculature, anti-VEGF therapies lead to an increase in hypoxia in the tumor microenvironment (41, 42). Emerging evidence suggests that therapy-induced hypoxia may be a contributing factor to the disappointing clinical results of anti-VEGF strategies (41, 42). Hypoxia, either in the transient or persistent state, is a hallmark of cancer. HIF-1α, the main mediator of hypoxia has been shown to regulate pathways involved in the maintenance of the cancer stem cell-like phenotype, angiogenesis and VM (27, 43, 44). Of note, melanomas with high VM capability also display increased HIF-1α expression levels (45). Here, we report that VEGF-A inhibition in WM1617 xenografts leads to a concomitant increase in VM and HIF-1α, suggesting that hypoxia-induced HIF-1α expression may be one important *in vivo* environmental cue promoting VM induction and MSLC maintenance (Fig. 6C) (27). Parallel to our findings, tumors from glioblastoma multiforme patients treated with bevacizumab, an anti-VEGF-A antibody, exhibit an increase in HIF-1α expression (46). Furthermore, daily administration of topotecan, a HIF-1α inhibitor, in combination with bevacizumab synergistically attenuates tumor growth and angiogenesis in a glioma xenograft model (47). Future work should further examine whether HIF-1α downregulation prevents the increase in VM induction and MSLC maintenance following VEGF-A inhibition in melanoma.

In summary, our work reveals that although VEGF-A silencing attenuates WM1617 cell growth *in vivo*, tumors compensate for VEGF-A knockdown by adopting VM, thereby promoting perivascular MSLC niche morphogenesis and MSLC enrichment potentially via a HIF-1α-mediated mechanism. In contrast, C8161 and A2058 cells are intrinsically resistant to VEGF-A silencing and, therefore, fail to show adaptive compensatory survival mechanisms. Our findings are critical in understanding the mechanisms of adaptive resistance in some melanomas following treatment with anti-VEGF agents. Future work should examine the specific signaling pathways involved in the adaptive response to VEGF-A inhibition. Uncovering the specific effectors of VM-induction and MSLC maintenance will be essential in discovering novel therapeutic targets to treat melanoma through combination therapies that simultaneously target angiogenesis and the MSLC niche.

Supplementary Material

Refer to Web version on PubMed Central for supplementary material.

Acknowledgments

Grant Support: This work was supported by the National Institutes of Health, National Cancer Institute (grant no. R01CA138649 to M-Y. Hsu).

References

1. Hanahan D, Weinberg RA. Hallmarks of cancer: the next generation. Cell. 2011; 144:646–674. [PubMed: 21376230]
2. Yancopoulos GD, Davis S, Gale NW, Rudge JS, Wiegand SJ, Holash J. Vascular-specific growth factors and blood vessel formation. Nature. 2000; 407:242–248. [PubMed: 11001067]
3. Zaki KA, Basu B, Corrie P. The role of angiogenesis inhibitors in the management of melanoma. Curr Top Med Chem. 2012; 12:32–49. [PubMed: 22196268]
4. Casanovas O, Hicklin DJ, Bergers G, Hanahan D. Drug resistance by evasion of antiangiogenic targeting of VEGF signaling in late-stage pancreatic islet tumors. Cancer Cell. 2005; 8:299–309. [PubMed: 16226705]
5. Bergers G, Hanahan D. Modes of resistance to anti-angiogenic therapy. Nat Rev Cancer. 2008; 8:592–603. [PubMed: 18650835]
6. Ebos JM, Lee CR, Cruz-Munoz W, Bjarnason GA, Christensen JG, Kerbel RS. Accelerated metastasis after short-term treatment with a potent inhibitor of tumor angiogenesis. Cancer Cell. 2009; 15:232–239. [PubMed: 19249681]
7. Dunleavey JM, Dudley AC. Vascular Mimicry: Concepts and Implications for Anti-Angiogenic Therapy. Curr Angiogenes. 2012; 1:133–138. [PubMed: 24729954]
8. Demou ZN, Hendrix MJ. Microgenomics profile the endogenous angiogenic phenotype in subpopulations of aggressive melanoma. J Cell Biochem. 2008; 105:562–573. [PubMed: 18655191]
9. van der Schaft DW, Seftor RE, Seftor EA, Hess AR, Gruman LM, Kirschmann DA, et al. Effects of angiogenesis inhibitors on vascular network formation by human endothelial and melanoma cells. J Natl Cancer Inst. 2004; 96:1473–1477. [PubMed: 15467037]
10. Hendrix MJ, Seftor EA, Hess AR, Seftor RE. Vasculogenic mimicry and tumour-cell plasticity: lessons from melanoma. Nat Rev Cancer. 2003; 3:411–421. [PubMed: 12778131]
11. Folberg R, Hendrix MJ, Maniotis AJ. Vasculogenic mimicry and tumor angiogenesis. Am J Pathol. 2000; 156:361–381. [PubMed: 10666364]
12. Paulis YW, Soetekouw PM, Verheul HM, Tjan-Heijnen VC, Griffioen AW. Signaling pathways in vasculogenic mimicry. Biochemim Biophys Acta. 2010; 1806:18–28.
13. Hess AR, Seftor EA, Gruman LM, Kinch MS, Seftor RE, Hendrix MJ. VE-cadherin regulates EphA2 in aggressive melanoma cells through a novel signaling pathway: implications for vasculogenic mimicry. Cancer Biol Ther. 2006; 5:228–233. [PubMed: 16481735]
14. Hendrix MJ, Seftor EA, Hess AR, Seftor RE. Molecular plasticity of human melanoma cells. Oncogene. 2003; 19(22):3070–3075. [PubMed: 12789282]
15. Seftor EA, Meltzer PS, Schatteman GC, Gruman LM, Hess AR, Kirschmann DA, et al. Expression of multiple molecular phenotypes by aggressive melanoma tumor cells: role in vasculogenic mimicry. Crit Rev Oncol Hematol. 2002; 44:17–27. [PubMed: 12398997]
16. Zabierowski SE, Herlyn M. Melanoma stem cells: the dark seed of melanoma. J Clin Oncol. 2008; 26:2890–2894. [PubMed: 18539969]
17. Fang D, Nguyen TK, Leishear K, Finko R, Kulp AN, Hotz S, et al. A tumorigenic subpopulation with stem cell properties in melanomas. Cancer Res. 2005; 65:9328–9337. [PubMed: 16230395]
18. Redmer T, Welte Y, Behrens D, Fichtner I, Przybilla D, Wruck W, et al. The Nerve Growth Factor Receptor CD271 Is Crucial to Maintain Tumorigenicity and Stem-Like Properties of Melanoma Cells. PLoS One. 2014; 9:e92596. [PubMed: 24799129]

19. Lai CY, Schwartz BE, Hsu MY. CD133^{+} Melanoma Subpopulations Contribute to Perivascular Niche Morphogenesis and Tumorigenicity through Vasculogenic Mimicry. Cancer Res. 2012; 72:5111–5118. [PubMed: 22865455]
20. Conley SJ, Gheordunescu E, Kakarala P, Newman B, Korkaya H, Heath AN, et al. Antiangiogenic agents increase breast cancer stem cells via the generation of tumor hypoxia. Proc Natl Acad Sci U S A. 2012; 109:2784–2789. [PubMed: 22308314]
21. Wang R, Chadalavada K, Wilshire J, Kowalik U, Hovinga KE, Geber A, et al. Glioblastoma stem-like cells give rise to tumour endothelium. Nature. 2010; 468:829–833. [PubMed: 21102433]
22. Hsu, MY.; Elder, DE.; Herlyn, M. The Wistar melanoma (WM) cell lines. In: Masters, J.; Palsson, B., editors. Human cell culture. Nowell: Kluwer publishers; 1999. p. 259-274.
23. Hsu MY, Rovinsky SA, Lai CY, Qasem S, Liu X, How J, et al. Aggressive melanoma cells escape from BMP7-mediated autocrine growth inhibition through coordinated Noggin upregulation. Lab Invest. 2008; 88:842–855. [PubMed: 18560367]
24. Zhan Y, Abi Saab WF, Modi N, Stewart AM, Liu J, Chadee DN. Mixed lineage kinase 3 is required for matrix metalloproteinase expression and invasion in ovarian cancer cells. Exp Cell Res. 2012; 318:1641–1648. [PubMed: 22652451]
25. Liu JW, Dunoyer-Geindre S, Blot-Chabaud M, Sabatier F, Fish RJ, Bounameaux H, et al. Generation of human inflammation-resistant endothelial progenitor cells by A20 gene transfer. J Vasc Res. 2010; 47:157–167. [PubMed: 19851077]
26. Livak KJ, Schmittgen TD. Analysis of relative gene expression data using real time quantitative PCR and the 2(-Delta Delta C(T)) Method. Methods (San Diego, Calif). 2001; 25:402–408.
27. Kirschmann DA, Seftor EA, Hardy KM, Seftor RE, Hendrix MJ. Molecular pathways: vasculogenic mimicry in tumor cells: diagnostic and therapeutic implications. Clin Cancer Res. 2012; 18:2726–2732. [PubMed: 22474319]
28. Meier F, Nesbit M, Hsu MY, Martin B, Van Belle P, Elder DE, et al. Human melanoma progression in skin reconstructs : biological significance of bFGF. Am J Pathol. 2000; 156:193–200. [PubMed: 10623667]
29. Yasushi S, Tomotoshi M, Dinorah FM, Mie S, Fei L, Hiroyuki M, et al. Transdifferentiation of glioblastoma cells into vascular endothelial cells. Proc Natl Acad Sci U S A. 2011; 108:4274–4280. [PubMed: 21262804]
30. Francescone R, Scully S, Bentley B, Yan W, Taylor SL, Oh D, Moral L, Shao R. Glioblastoma-derived tumor cells induce vasculogenic mimicry through Flk-1 protein activation. J Biol Chem. 2012; 287:24821–24831. [PubMed: 22654102]
31. Mei J, Gao Y, Zhang L, Cai X, Qian Z, Huang H, Huang W. VEGF-siRNA silencing induces apoptosis, inhibits proliferation and suppresses vasculogenic mimicry in osteosarcoma in vitro. Exp Oncol. 2008; 30:29–34. [PubMed: 18438338]
32. Yao X, Ping Y, Liu Y, Chen K, Yoshimura T, Liu M, Gong W, Chen C, Niu Q, Guo D, Zhang X, Wang JM, Bian X. Vascular endothelial growth factor receptor 2 (VEGFR-2) plays a key role in vasculogenic mimicry formation, neovascularization and tumor initiation by Glioma stem-like cells. PLoS One. 2013; 8(3):e57188. [PubMed: 23536763]
33. Scully S, Francescone R, Faibish M, Bentley B, Taylor SL, Oh D, Schapiro R, Moral L, Yan W, Shao R. Transdifferentiation of glioblastoma stem-like cells into mural cells drives vasculogenic mimicry in glioblastomas. J Neurosci. 2012; 32:12950–12960. [PubMed: 22973019]
34. Frank NY, Schatton T, Kim S, Zhan Q, Wilson BJ, Ma J, Saab KR, Osherov V, Widlund HR, Gasser M, Waaga-Gasser AM, Kupper TS, Murphy GF, Frank MH. VEGFR-1 expressed by malignant melanoma-initiating cells is required for tumor growth. Cancer Res. 2011; 71:1474–1485. [PubMed: 21212411]
35. Fukunaga-Kalabis M, Roesch A, Herlyn M. From cancer stem cells to tumor maintenance in melanoma. J Invest Dermatol. 2011; 131:1600–1604. [PubMed: 21654838]
36. Velazquez OC, Herlyn M. The vascular phenotype of melanoma metastasis. Clin Exp Metastasis. 2003; 20:229–235. [PubMed: 12741681]
37. Valyi-Nagy K, Kormos B, Ali M, Shukla D, Valyi-Nagy T. Stem cell marker CD271 is expressed by vasculogenic mimicry-forming uveal melanoma cells in three-dimensional cultures. Mol Vision. 2012; 18:588–592.

38. Barcellos-Hoff MH, Newcomb EW, Zagzag D, Narayana A. Therapeutic targets in malignant glioblastoma microenvironment. Semin Radiat Oncol. 2009; 19:163–170. [PubMed: 19464631]
39. Wurmser AE, Palmer TD, Gage FH. Neuroscience. Cellular interactions in the stem cell niche. Science (New York, NY). 2004; 304:1253–1255.
40. Moore KA, Lemischka IR. Stem cells and their niches. Science (New York, NY). 2006; 311:1880–1885.
41. Blagosklonny MV. Antiangiogenic therapy and tumor progression. Cancer Cell. 2004; 5:13–17. [PubMed: 14749122]
42. Kerbel R, Folkman J. Clinical translation of angiogenesis inhibitors. Nat Rev Cancer. 2002; 2:727–739. [PubMed: 12360276]
43. Seftor RE, Hess AR, Seftor EA, Kirschmann DA, Hardy KM, Margaryan NV, et al. Tumor cell vasculogenic mimicry: from controversy to therapeutic promise. Am J Pathol. 2012; 181:1115–1125. [PubMed: 22944600]
44. Postovit LM, Seftor EA, Seftor RE, Hendrix MJ. Influence of the microenvironment on melanoma cell fate determination and phenotype. Cancer Res. 2006; 66:7833–7836. [PubMed: 16912153]
45. Sun B, Zhang D, Zhang S, Zhang W, Guo H, Zhao X. Hypoxia influences vasculogenic mimicry channel formation and tumor invasion-related protein expression in melanoma. Cancer Lett. 2007; 249:188–197. [PubMed: 16997457]
46. Iwamoto FM, Abrey LE, Beal K, Gutin PH, Rosenblum MK, Reuter VE, et al. Patterns of relapse and prognosis after bevacizumab failure in recurrent glioblastoma. Neurology. 2009; 73:1200–1206. [PubMed: 19822869]
47. Rapisarda A, Hollingshead M, Uranchimeg B, Bonomi CA, Borgel SD, Carter JP, et al. Increased antitumor activity of bevacizumab in combination with hypoxia inducible factor-1 inhibition. Mol Cancer Ther. 2009; 8:1867–1877. [PubMed: 19584228]
48. Vartanian A, Gatsina G, Grigorieva I, Solomko E, Dombrovsky V, Baryshnikov A, et al. The involvement of Notch signaling in melanoma vasculogenic mimicry. Clin Exp Med. 2013; 13:201–209. [PubMed: 22627943]

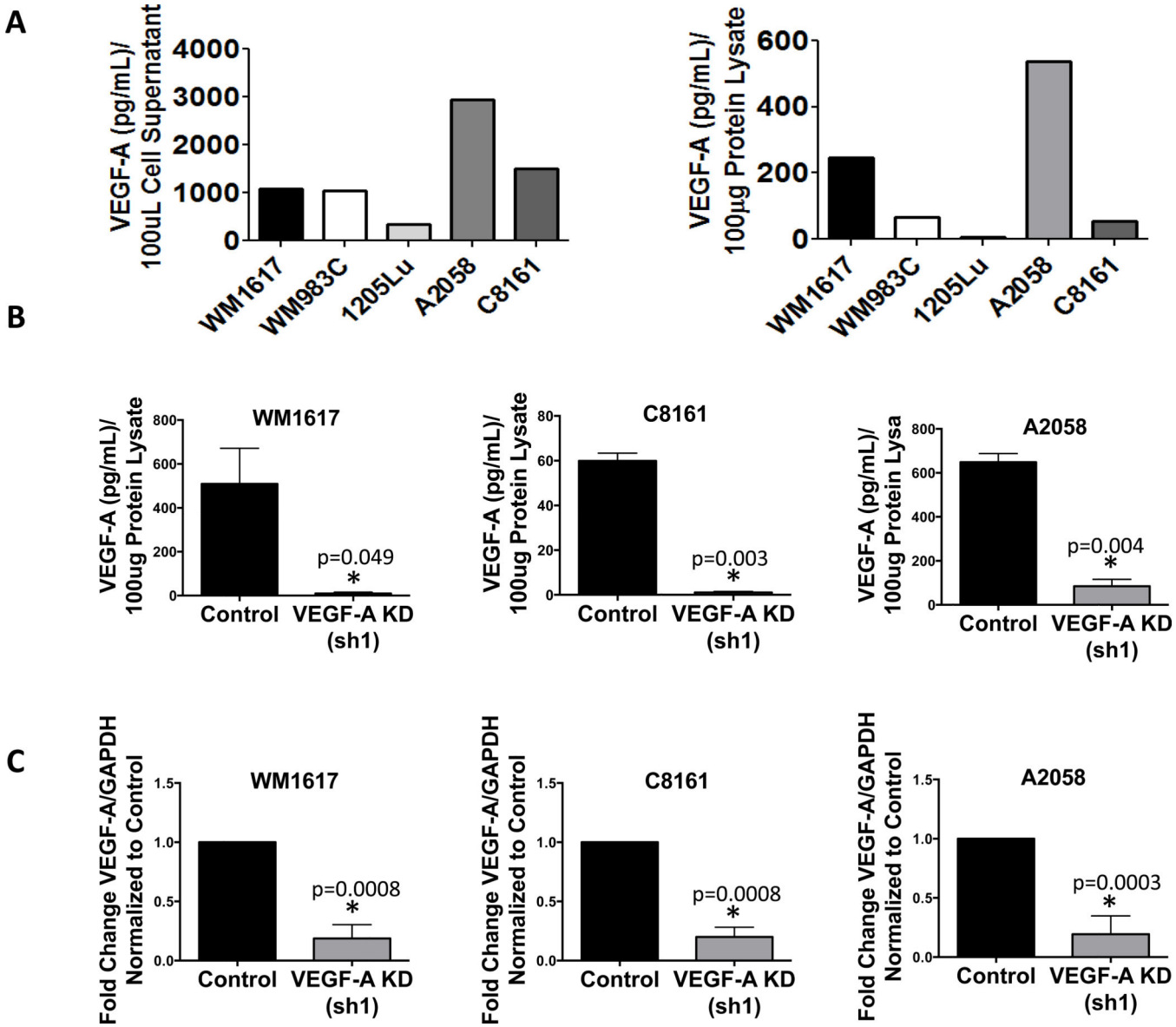

Figure 1. VEGF-A silencing in WM1617, C8161 and A2058 melanoma cells by plasmid-based shRNA

A, VEGF-A expression was examined in the cell supernatants of a panel of melanoma cells, including WM1617, WM983C, 1205Lu, A2058, and C8161 cells (left panel). VEGF-A expression was confirmed in 100 µg of protein lysates harvested from WM1617, WM983C, 1205Lu, A2058, and C8161 cells (right panel). WM1617, C8161 and A2058 cells displayed the highest VEGF-A expression. B, VEGF-A KD in 100 µg of protein lysates harvested from WM1617, C8161 and A2058 cells stably transfected with nontarget control or VEGF-A shRNA (sh1) was confirmed using a human VEGF-A ELISA kit. *, P<0.05. C, qRT-PCR confirmed VEGF-A downregulation in WM1617, C8161 and A2058 VEGF-A KD (sh1) cells compared to nontarget controls. *, P<0.05.

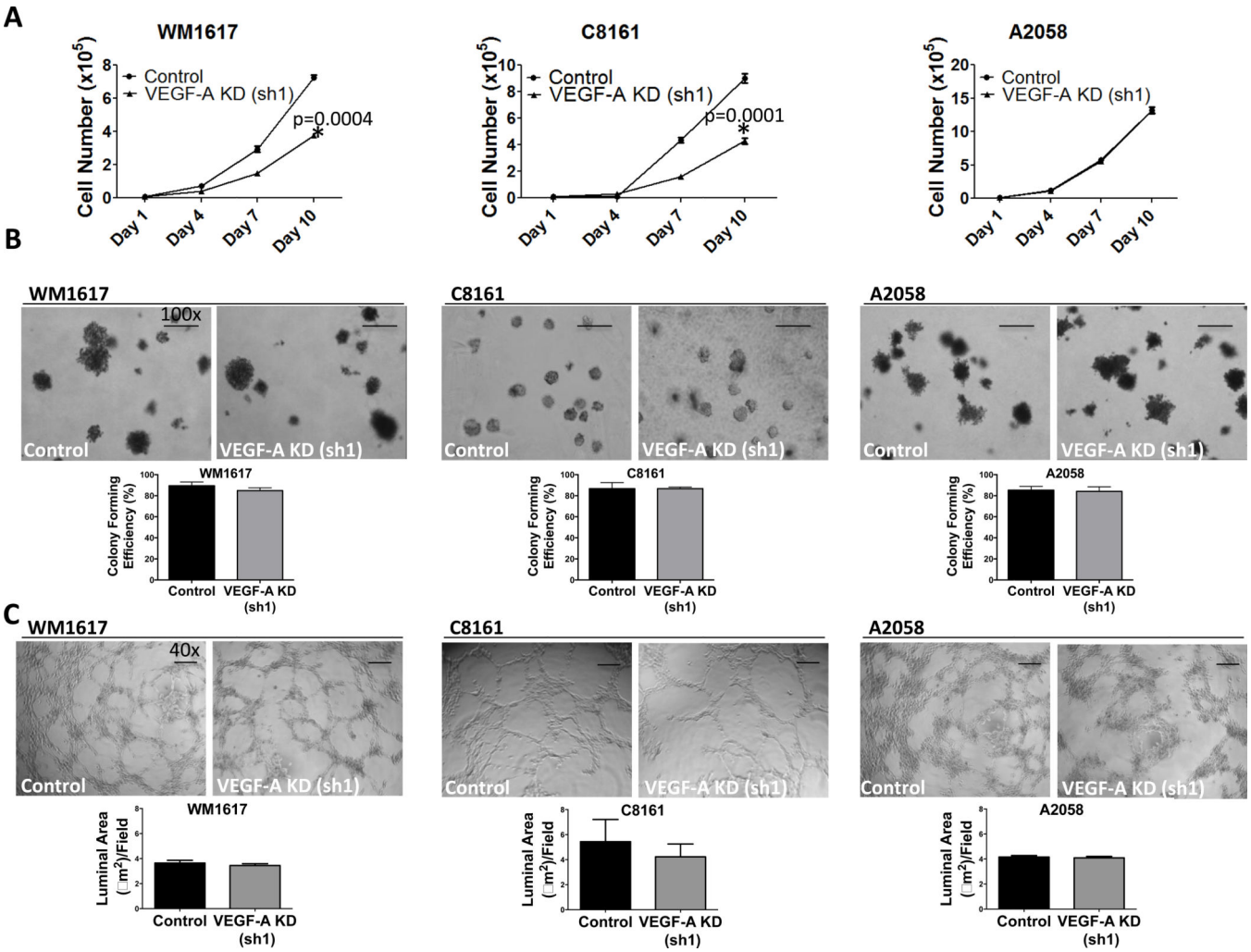

Figure 2. VEGF-A KD attenuates WM1617 and C8161 but not A2058 melanoma cell growth *in vitro*

A, 2D Growth assays revealed that VEGF-A KD (sh1) inhibited WM1617 and C8161, but not A2058 melanoma cell growth *in vitro*. *, P<0.05. B, No change in colony formation was observed following VEGF-A KD (sh1) in WM1617, C8161 or A2058 melanoma cells. Data shown represent average percentage clonogenicity from three different experiments. Magnification, 100×. Scale bar: 500 μm. C, No change in vasculogenic mimicry as determined by tubule formation on matrigel per field was observed in WM1617, C8161 or A2058 VEGF-A KD (sh1) cells compared to controls *in vitro*. Magnification, 40×. Scale bar: 1 μm.

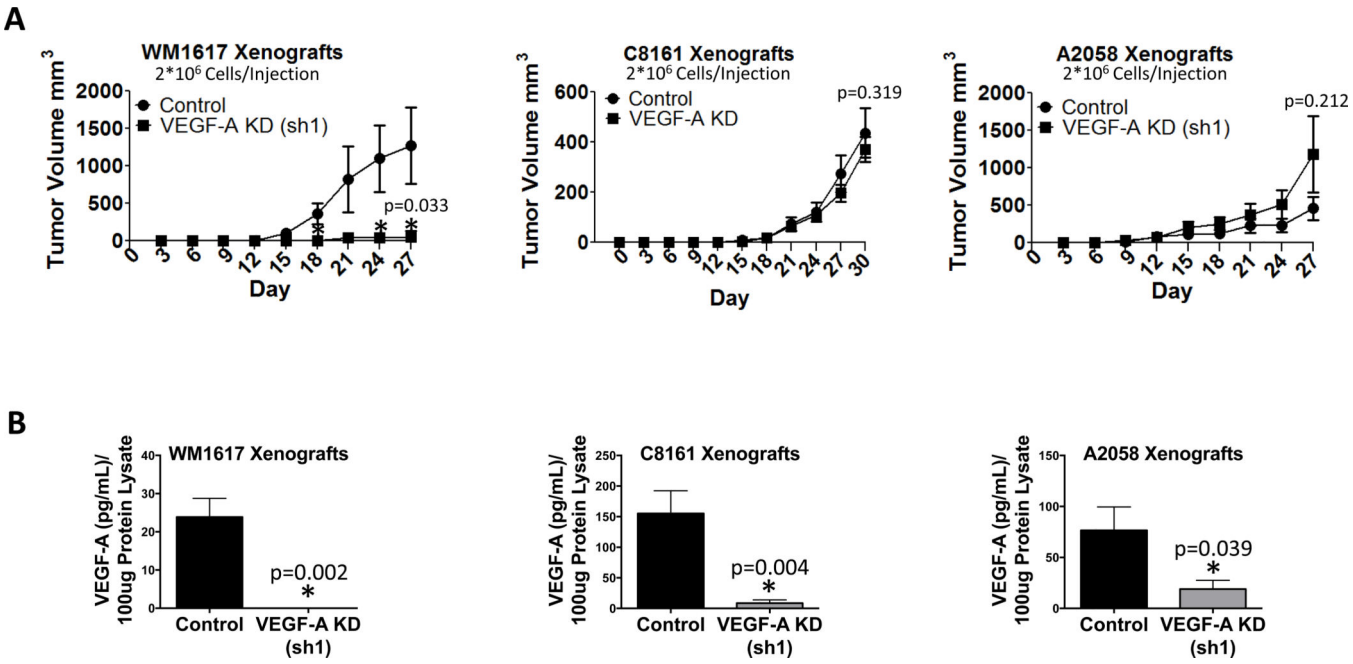

Figure 3. VEGF-A KD retards tumorigenicity in WM1617 but not C8161 or A2058 melanoma xenografts

A, Tumorigenicity assays revealed that VEGF-A KD (sh1) in WM1617 (A, left panel, *n*=5, 2 × 10^6 cells/mouse) resulted in significant growth inhibition *in vivo*. *, P<0.05. No growth alteration was observed in C8161 (A, middle panel, *n*=5, 2 × 10^6 cells/mouse) or A2058 (A, right panel, *n*=5, 2 × 10^6 cells/mouse) melanoma cell xenografts expressing VEGF-A shRNA (sh1) compared to nontarget control shRNA *in vivo*. B, VEGF-A KD in 100 μg of protein homogenates harvested from WM1617, C8161 and A2058 xenografts expressing nontarget control or VEGF-A shRNA (sh1) was confirmed using a human VEGF-A ELISA kit (n=5). *, P<0.05.

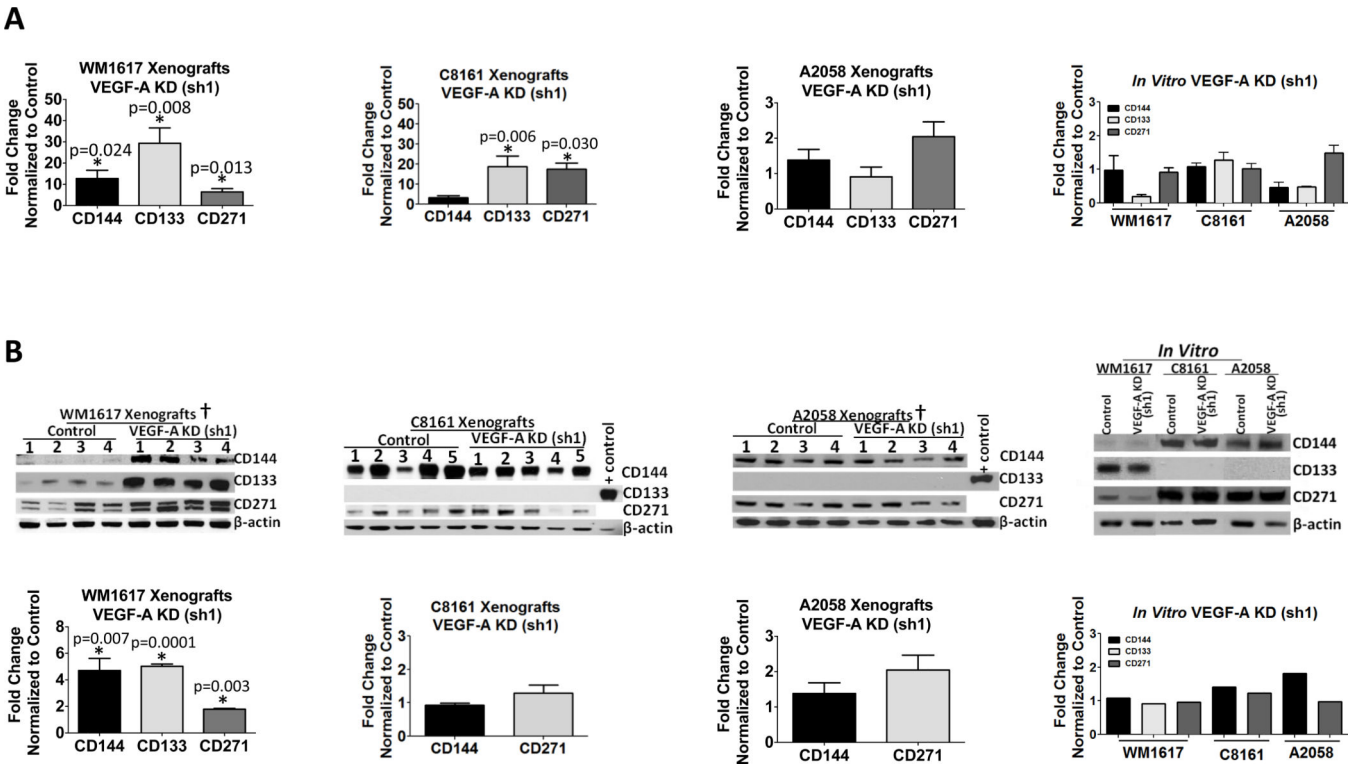

Figure 4. VEGF-A KD increases VM and MSLC markers in WM1617 melanoma xenografts

A, Expression profiling by qRT-PCR revealed concomitant CD144, CD133 and CD271 upregulation in WM1617 VEGF-A KD (sh1) xenografts compared to nontarget controls. A concomitant increase in CD133 and CD271, but not CD144 was also observed in C8161 VEGF-A KD (sh1) xenografts compared to nontarget controls. No change in CD144, CD133 or CD271 expression was observed in A2058 VEGF-A KD (sh1) xenografts compared to nontarget controls. No change in these markers was observed in WM1617, C8161 or A2058 VEGF-A KD (sh1) cells compared to nontarget controls *in vitro*. *, P<0.05. B, Cell lysates (the forth panel) and xenograft homogenates (the first three panels) prepared from WM1617, C8161 and A2058 VEGF-A KD (sh1) and nontarget control melanoma cells were subjected to Western blotting. β-actin served as internal loading control. A significant increase in CD144, CD133 and CD271 was observed in WM1617 VEGF-A KD (sh1) xenografts compared with the nontarget controls (far left upper panel) as determined by densitometry (far left lower panel); no change in these markers was observed in WM1617 VEGF-A KD (sh1) cells compared to nontarget controls *in vitro* (far right panel). *, P<0.05. No change in CD144 or CD271 expression was observed in C8161 or A2058 VEGF-A KD (sh1) xenografts (middle panels) or cells *in vitro* (far right panel) compared to nontarget controls. Unfortunately, despite maximal loading (100 μg protein per lane) and prolonged exposure (overnight), the expression of CD133 was under the detection limit in both C8161 and A2058 xenografts and cells *in vitro* (WM1617 lysate was included as a positive control). †Four out of five xenograft pairs generated were examined by Western blotting as one xenogaft pair was depleted for histological evaluation, including multilabel IF and fixed paraffin preparation.

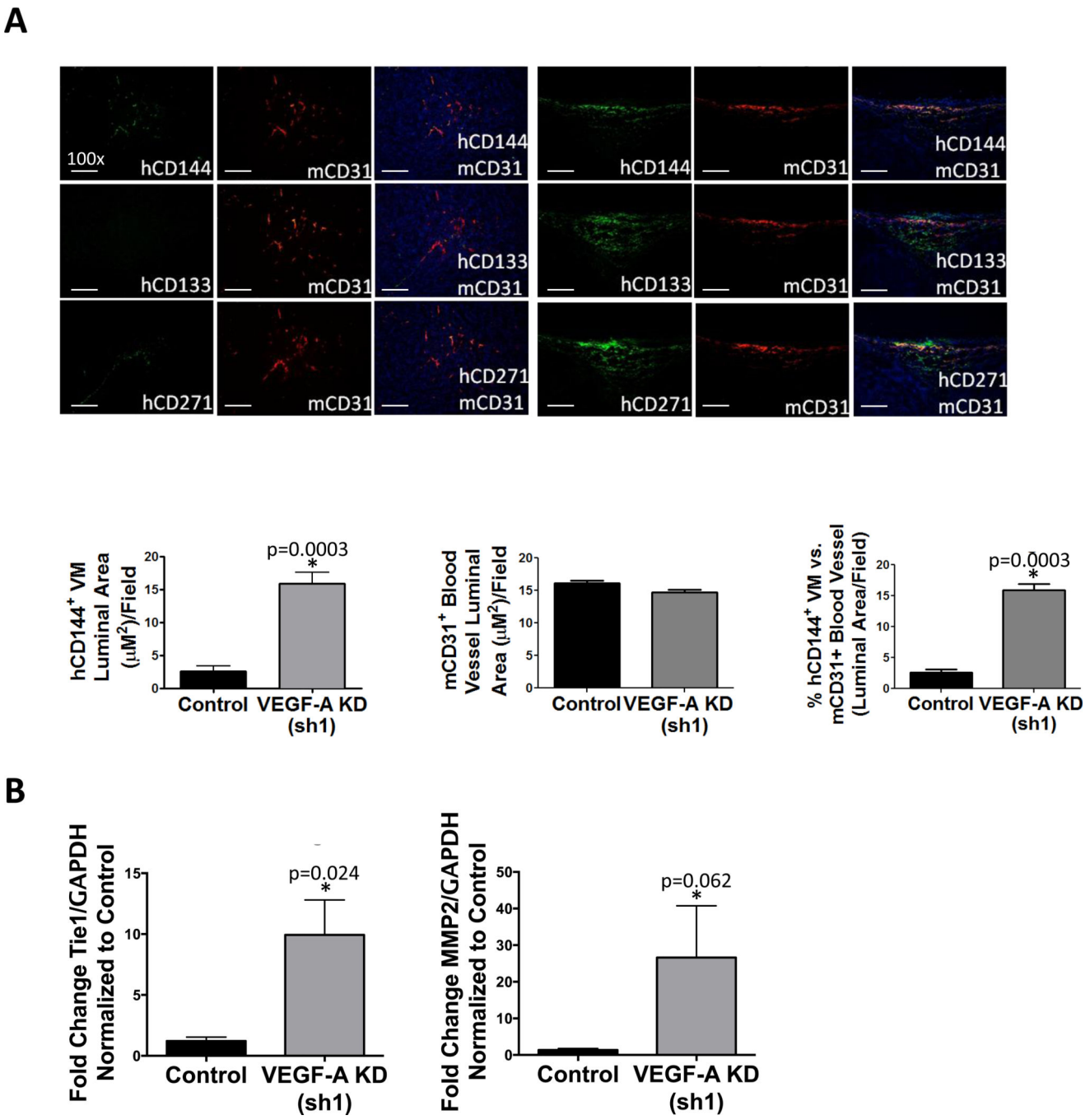

Figure 5. VEGF-A KD promotes VM and enriches MSLCs in WM1617 melanoma xenografts

A, IF analysis of consecutive WM1617 xenograft sections double labeled for mCD31$^+$ host blood vessels showed that WM1617 VEGF-A KD (sh1) xenografts displayed increased VM-engaging melanoma cells (hCD144$^+$ in green; top panel) in close physical proximity to hCD133$^+$ MSLCs (in green; middle panel) and hCD271$^+$ MSLCs (in green; bottom panel) compared to nontarget control xenografts. Magnification, 100×. Scale bar: 200 μm. Human melanoma-derived VM vessels (hCD144$^+$) and host angiogenesis (mCD31$^+$) and were quantified as measured by the average luminal area per 100× field and revealed a significant

increase in hCD144^{+} VM luminal area in WM1617 VEGF-A KD (sh1) xenografts compared to controls (left panel), no change in mCD31^{+} luminal area of host blood vessels (middle panel), and a significant increase in the percentage of melanoma VM channels (hCD144^{+}) compared to mCD31^{+} blood vessels. *, $P<0.05$. C, Expression profiling by qRT-PCR revealed concomitant Tie-1 and MMP-2 upregulation in WM1617 VEGF-A KD (sh1) xenografts compared to nontarget controls. *, $P<0.05$.

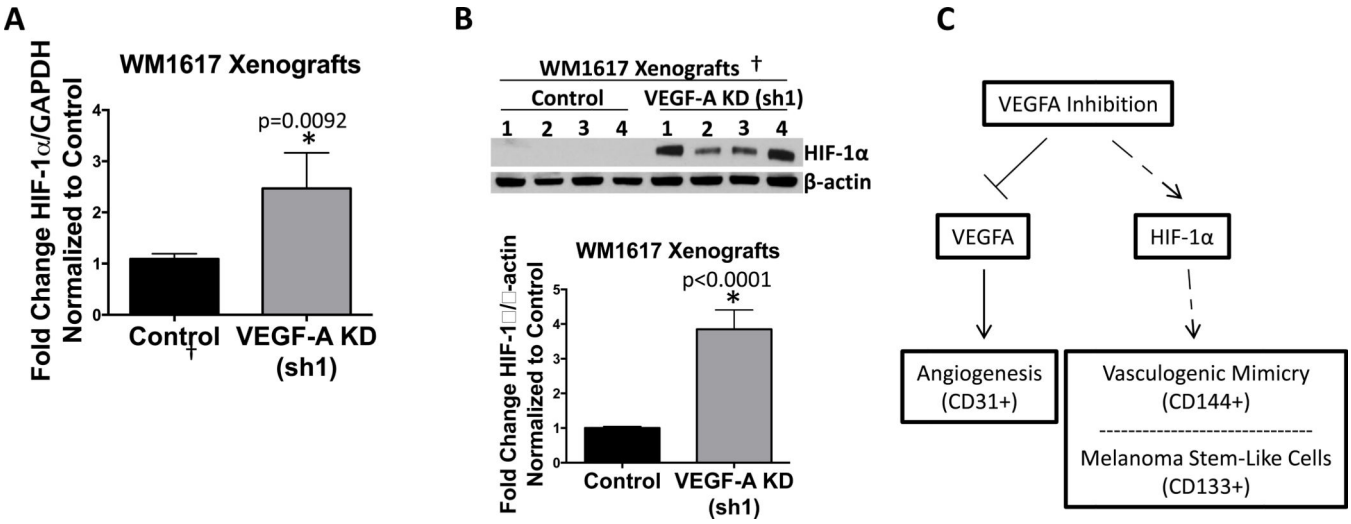

Figure 6. HIF-1α is upregulated in WM1617 VEGF-A KD xenografts

A, Expression profiling by qRT-PCR revealed HIF-1α upregulation in WM1617 VEGF-A KD (sh1) xenografts compared to nontarget controls. *, P<0.05. B, Western blotting confirmed HIF-1α upregulation in WM1617 VEGF-A KD (sh1) xenografts compared to nontarget controls. β-actin served as internal loading control. †Four out of five xenograft pairs generated were examined by Western blotting as one xenogaft pair was depleted for histological evaluation, including multilabel IF and fixed paraffin preparation.

C, Proposed model of the adaptive response to VEGF-A inhibition. VEGF-A stimulates vascularization of tumors via angiogenesis. Following VEGF-A inhibition, HIF-1α is increased and, in turn, promotes: 1) VM, an alternative vascularization mechanism; and 2) MSLC enrichment.